Catalysis Letters (2021) 151:2366–2375
https://doi.org/10.1007/s10562-020-03469-5

Ionic Liquid-Assisted Synthesis of Vanadium Phosphate Catalysts from Phosphorous Acid for Selective Oxidation Reactions

Yu Zhao[1] · Weiwei Zhang[1] · Shidong Wang[1] · Peng Dong[1] · Guixian Li[1] · Jianyi Shen[2]

Received: 15 September 2020 / Accepted: 13 November 2020 / Published online: 2 January 2021

Abstract

Vanadium oxyphosphate (VPO) with a high surface area was synthesized in a mixed solvent of ionic liquid [Bmim]Br and water, using phosphorous acid to reduce V^{5+} to V^{4+} and as a partial phosphorus source, and V_2O_5 as the vanadium source. The effects of ionic liquids on the synthesis process were investigated in detail. Using pure water as the solvent, the product was a vanadium phosphate compound with large flakes. With the increase in the amount of ionic liquid, the size of the large flakes of vanadium phosphate gradually decreased, and the morphology was changed to spherical particles. When the proportion of ionic liquid was 80% or the ionic liquid was solely used as the solvent, the VPO showed completely spherical particle morphology, and the specific surface area was the highest. X-ray diffraction analysis showed that the crystal phase of VPO changed from vanadium (IV) hydrogenphosphate hemihydrate ($VOHPO_4{\cdot}0.5H_2O$) to an amorphous state with an increase in ionic liquid ratio. All of the above results show that ionic liquids play an important role in the synthesis of VPO materials. After being calcined in an n-butane/air atmosphere, the precursors were transformed into the vanadium pyrophosphate phase. The active VPO catalysts were used in the selective oxidation of cyclohexanol, and the yield of cyclohexanone was 57.98% for the VPO-80 catalyst synthesized using the ionothermal method but only 21.41% for the VPO-W catalyst synthesized using a traditional hydrothermal method, which shows the advantage of ionic liquid synthesis for VPO catalysts.

Graphic Abstract

Vanadium oxyphosphate material with high surface area was synthesized in the mixed solvent of ionic liquid [Bmim]Br and water. Ionic liquid plays an important role in the morphology and properties of synthesized VPO materials. The active VPO catalysts were used in the selective oxidation of cyclohexanol, and the yield of cyclohexanone was 57.98% for VPO-80 catalyst synthesized by ionothermal method, but only 21.41% for VPO-W catalyst synthesized by traditional hydrothermal method, which exhibited the advantages of ionic liquid synthesis for VPO catalysts.

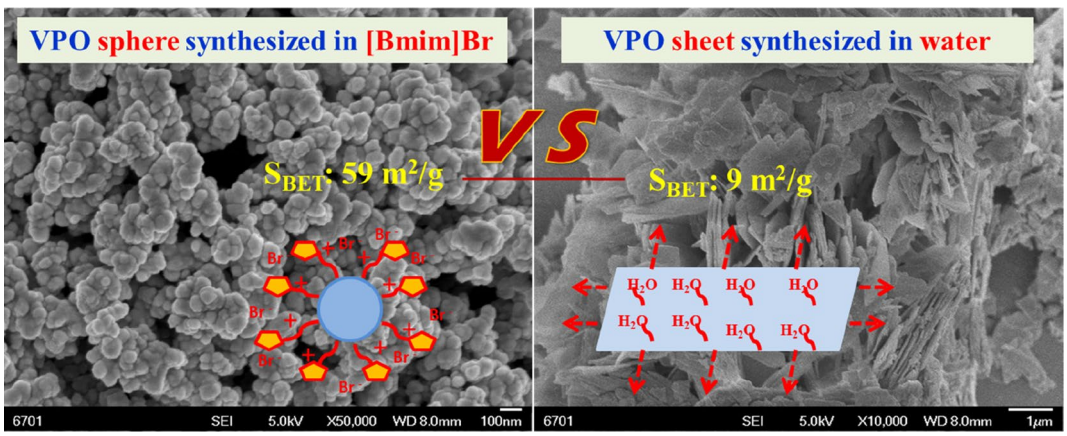

Keywords Vanadium phosphate · Ionothermal synthesis · Phosphorous acid · Oxidation reactions · Cyclohexanone

Extended author information available on the last page of the article

1 Introduction

Vanadium-based phosphate catalysts have been widely studied since the 1960s [1]. Because of their rich and complex structural chemistry characteristics, vanadium-based phosphate materials have been widely used in selective alkane oxidation reactions [2, 3], especially in C2–C4 selective alkane oxidation [4], dehydration [5] and other low-temperature liquid-phase reactions [6]. The catalytic oxidation of n-butane to maleic anhydride by vanadium oxyphosphate (VPO) catalyst is one of the classic examples [7–9]. So far, no better catalyst has been found to replace it in industry [10–12].

Up to now, the preparation of vanadium-based phosphate materials mainly includes the synthesis of precursor vanadium (IV) hydrogenphosphate hemihydrate ($VOHPO_4{\cdot}0.5H_2O$) by a hydrothermal or alcohol solvothermal method and then roasting in air containing about 1.5% n-butane to obtain the final catalyst, vanadium pyrophosphate [12, 13]. The morphology and specific surface area of the precursor directly determine the texture parameters and catalytic performance of the final catalyst. Therefore, the synthesis of VPO catalysts is mainly focused on the preparation of the precursor. According to the literature, the precursor $VOHPO_4{\cdot}0.5H_2O$, is usually formed from vanadium pentoxide and phosphoric acid in the presence of a reducing agent. The V^{5+} can be effectively reduced to V^{4+} by a good reducing agent, and then forms a VPO precursor with a clear crystal phase (such as $VOHPO_4{\cdot}0.5H_2O$) with phosphate ion. It includes the following routes: (1) VPA route [14]. In this method, water is used as the solvent and hydrochloric acid as the reducing agent to prepare $VOHPO_4{\cdot}0.5H_2O$. Later, different reducing agents are used, such as lactic acid and oxalic acid. The precursor synthesized by this route is characterized by large irregular morphology, low specific surface area (≈ 3 m^2/g) and a large amount of impurity $VO(H_2PO_4)_2$. (2) VPO route [13, 15]. In this method, alcohols are used as the solvent and reducing agent to prepare $VOHPO_4{\cdot}0.5H_2O$ in one pot. The surface area of the precursor is also increased, but it is still very low (≈ 10 m^2/g). (3) VPD route [12, 16, 17]. $VOPO_4{\cdot}2H_2O$ is prepared from phosphoric acid and V_2O_5 with water as the solvent and then refluxed in an alcohol solution to obtain $VOHPO_4{\cdot}0.5H_2O$. The specific surface area of the precursor prepared by this route is increased (≈ 30 m^2/g), but the steps are complex, being a two-step synthesis. (4) Other methods. By adding an organic template (piperazine), $NaVO_3$, vanadium and H_3PO_4 solution are mixed and crystallized at 170 °C for 7 days to obtain mesoporous VPO. The disadvantage of this method is that the reaction temperature is high and considerable time is needed [18]. Otaibi et al. [19] found the method of adding $VOHPO_4{\cdot}0.5H_2O$ can greatly improve the yield of synthetic materials and reduce the generation of impurity $VO(H_2PO_4)_2$, but the specific surface area of the catalyst is still very low, and the synthesis process is complex.

Hutchings et al. [20] reported that the precursor of VPO can be successfully prepared using H_3PO_3 as a reducing agent in aqueous solution. In this method, phosphite ion is not only used as a reducing agent but also as a phosphorus source, which greatly simplifies the reaction process. The precursor, $VOHPO_4{\cdot}0.5H_2O$, can be synthesized in one step. However, the specific surface area of the vanadium phosphate precursor prepared by this method is low (< 15 m^2/g), which greatly affects subsequent catalytic activity.

The preparation of inorganic materials using ionic liquids as a solvent has attracted much attention in recent years [21]. Many new materials, such as aluminum phosphate molecular sieves [21, 22], zirconium phosphate [23], metal-organic frameworks [24], metal oxides [25], metal sulfides [26], metal vanadate [27], metal chloride [28, 29] or metal boride [30], are prepared by ionothermal synthesis or ionic-liquid-assisted synthesis. Ionic liquids have many advantages over traditional aqueous or organic solvents [31]. For example, it is not only a solvent but also a template, which makes the reaction system simpler. There are many kinds of ionic liquids that can synthesize nanomaterials with different properties or morphologies; there is almost no saturated vapor pressure, so they can be synthesized under normal pressure, which makes the operation safe and easy. Therefore, academic research in this field has been carried out enthusiastically.

The synthesis of cyclohexanone by catalytic oxidation of cyclohexanol is an important industrial reaction [32]. Cyclohexanone is an important organic chemical raw material and industrial solvent, and the main intermediate for the production of nylon, caprolactam and adipic acid. The new reaction process with VPO as the catalyst and H_2O_2 as the oxidant has the advantages of environmental friendliness and low production cost.

In this paper, a series of VPO catalysts was successfully prepared using ionic liquid or a mixture of ionic liquid and water as the solvent, phosphorous acid as reducing agent and phosphorus source, and V_2O_5 as the vanadium source. With the addition of ionic liquids, the specific surface area of the synthesized materials increased significantly, and the morphology changed greatly, indicating the important influence of ionic liquids in the synthesis process. The vanadium pyrophosphate catalyst calcined in an n-butane/air atmosphere was used in the probe reaction of cyclohexanol oxidation to cyclohexanone, which performed differently compared with the catalyst synthesized in aqueous solution, possibly with higher specific surface area and different morphology effects.

2 Experiment

2.1 Preparation of Materials

The ionic liquid [Bmim]Br was prepared according to [33]. Bromobutane (250 g) and 100 g of *N*-methylimidazole were in turn added to a 500 ml four-neck flask containing a serpentine condenser tube, stirring rod, N_2 inlet and thermometer. The four-neck flask was placed in a water bath and maintained at 50 °C for 5 h under N_2, then cooled to room temperature. The reaction mixture was washed three times with ethyl acetate and vacuum dried at 70 °C for 3 h.

A mixture of ionic liquid and water in different proportions was used as the solvent in this work, V_2O_5 as the vanadium source, phosphorous acid as the reducing agent and part of the phosphorus source, and phosphoric acid was used as an additional phosphorus source, so that the system had a sufficient P/V ratio required for the synthesis of the $VOHPO_4{\cdot}0.5H_2O$ crystalline phase VPO precursor. The function of the autoclave was to ensure that the temperature of the reaction mixture reached about 150 °C in the presence of water. According to Hutchings' study, the VPO precursor of the $VOHPO_4{\cdot}0.5H_2O$ crystal phase must be synthesized above 145 °C when phosphite is used as a reducing agent.

Specifically, 5.9 g (0.032 mol) V_2O_5, 4.1 g (0.050 mol) H_3PO_3 and 2.2 g (0.019 mol) 85% H_3PO_4 were successively added to six 50-ml single port flasks. To flask No. 1, 22 ml of deionized water was added. To flask No. 2, 17 ml of deionized water and 5 ml of ionic liquid were added. To flask No. 3, 13 ml of deionized water and 9 ml of ionic liquid were added. To flask No. 4, 9 ml of deionized water and 13 ml ionic liquid were added. To flask No. 5, 4 ml of deionized water and 18 ml of ionic liquid were added. Finally, to flask No. 6, 22 ml of ionic liquid was added. The mixture was stirred at 60 °C for 5 h to dissolve the solid powder and then transferred to a hydrothermal autoclave at 150 °C for 72 h. After the reaction, the autoclave was cooled to room temperature. The solid obtained was washed with deionized water and absolute ethanol several times, and then dried at 80 °C for 12 h. The obtained VPO catalyst precursors were named as follows: VPO-pre-0, VPO-pre-20, VPO-pre-40, VPO-pre-60, VPO-pre-80 and VPO-pre-100. After calcination of the precursor at 400 °C in a 1.2% n-butane/air atmosphere for 15 h, the final catalysts were named VPO-W, VPO-20, VPO-40, VPO-60, VPO-80 and VPO-IL.

2.2 Characterization of Materials

N_2 adsorption–desorption measurements were carried out at 77 K using a Micromeritics Gemini V 2380 autosorption analyzer. The specific surface areas were calculated according to the Brunauer–Emmett–Teller (BET) equation while the pore distributions were obtained using the Barret–Joyner–Halenda (BJH) method. Samples were degassed in flowing N_2 at 200 °C for 5 h before the measurements.

X-ray diffraction (XRD) patterns were collected on a Shimadzu XRD-6000 powder diffractometer (Japan) using Cu Kα radiation ($\lambda = 0.1541$ nm). The 2θ scans covered the range of 10° to 80° with a step size of 0.02°.

Scanning electron microscopy (SEM) was carried out using a JEOL-JSM-6700F electron microscope. The samples were coated with gold using a sputter coater.

The average oxidation states of vanadium and nickel in the samples were studied using X-ray photoelectron spectroscopy (XPS) on a Thermo ESCALAB 250 spectrometer with monochromatic Al Kα radiation ($h\nu = 1486.6$ eV) operating at 150 W with a 500 μm diameter analysis area and a pass energy of 20 eV. The binding energies (BEs) for sample charging were calibrated using the C 1 s peak at 284.8 eV.

2.3 Catalytic Tests

The catalytic experiments were carried out in a round-bottom 25 ml glass flask reactor equipped with a reflux condenser and a magnetic stirrer at 343 K. In a typical experiment, $C_6H_{11}OH$ (2.00 g) was mixed in the three-neck flask with MeCN (10 ml) and VPO catalyst (0.2 g). After heating for 5 min under stirring, H_2O_2 (30%) was injected to start the oxidation reaction. The reaction was carried out for different times under atmospheric pressure. Then, the reaction mixture was naturally cooled to room temperature and filtered to separate the catalyst. The filtrate was analyzed on an SP-3420 gas chromatograph equipped with a flame ionization detector and an SE-54 capillary column (0.32 mm × 0.5 μm × 30 m), using the internal standard method with toluene as the standard substance to determine the amount of cyclohexanol and cyclohexanone, and other byproducts (mainly adipic acid) were not analyzed one by one, but directly summarized into "others". The conversion of cyclohexanol and selectivity of cyclohexanone were calculated based on the following equations:

$$\text{Cyclohexanol Conversion}(\%) = 100 - \frac{\text{Amount of cyclohexanol after reaction (mol)}}{\text{Total amount of cyclohexanol in the feed (mol)}} \times 100$$

$$\text{Cyclohexanone Selectivity}\,(\%) = \frac{\text{Amount of cyclohexanone (mol)}}{\text{Total amount of cyclohexanol converted (mol)}} \times 100$$

3 Results and Discussion

3.1 SEM

The SEM images of the catalyst precursor are shown in Fig. 1, with (a) VPO-pre-100, (b) VPO-pre-80, (c) VPO-pre-60, (d) VPO-pre-40, (e) VPO-pre-20 and (f) VPO-pre-0. The results show that the precursor synthesized in pure water (VPO-pre-0) had a large flaky morphology, which is consistent with the literature [20]. When the ionic liquid ratio was less than 60%, all the VPO catalyst precursors contained sheet-like structure morphology, which is a mixture of flakes and spheres at 60%, while the morphology of catalyst precursors synthesized at 80% or pure ionic liquid (100%) completely transformed into uniformly spherical particles. With an increase in the proportion of ionic liquid, the morphology of the VPO catalyst precursor changed from large flakes to relatively small spheres, which indicated that ionic liquids had a great influence on the morphology of the materials. The effect of ionic liquids on vanadium and phosphorus ions is different from that of an aqueous solution, so it will affect the growth direction of each crystal face of the material, thus obtaining the difference between flakes and spheres. With the increase in ionic liquid content, the morphology of the material changed greatly at 60% and 80%, which also indicates that there was a critical point in this region, and the quantitative change is the embodiment of a qualitative change.

3.2 *N_2 Adsorption–Desorption Measurements*

BET surface areas and BJH pore distributions of the samples were obtained through adsorption–desorption measurements of N_2 at 77 K. Table 1 summarizes the surface areas, pore volumes and average pore diameters of VPO catalyst precursors and the final catalysts after calcination. The specific surface area of the catalyst precursor synthesized in pure water solvent (VPO-pre-0) was 9 m^2/g. When the amount of ionic liquid was 20% or 40%, the specific surface areas of the materials were 13 m^2/g and 12 m^2/g, respectively, similar to those synthesized in pure water. It can be seen from the electron microscope images that they are basically large flaky materials. When the content of ionic liquid was 60%, the specific surface area was greatly increased to 24 m^2/g. The morphology of the material was a mixture of flakes and spherical particles, as seen in Fig. 1c. Thus, we surmised that smaller spherical particles were the reason for the increase in specific surface area. When the amount of ionic liquid was further increased to 80% or 100% (pure ionic liquid), the specific surface area reached the maximum area, which was 59 m^2/g and 33 m^2/g, respectively. From the SEM images, the morphology of the materials (VPO-pre-80 and VPO-pre-100) completely transformed into small spherical particles, which supports the inference that the specific surface area was significantly increased due to small spherical particles being formed. The specific surface area of the VPO-pre-100 sample was lower than that of VPO-pre-80, and the particle size of the spherical particles of VPO-pre-80 was smaller than that of VPO-pre-100 from the SEM images. This indicates that the presence of an appropriate amount of water can make VPO material disperse better in the solvent system; thus, the particle size of VPO-pre-80 was smaller and the specific surface area was larger. After calcination of VPO-pre-80 and VPO-pre-100 precursors in an air mixture containing 1.2% n-butane at high temperature, the specific surface areas of the final VPO catalysts were 34 m^2/g and 24 m^2/g, respectively. The specific surface areas of samples decreased after calcination, which may be due to the structural change caused by the removal of crystal water and the agglomeration of particles.

The N_2 adsorption–desorption isotherms and pore size distribution curves for the VPO-pre-80 and VPO-pre-100 samples are shown in Fig. 2a. Both samples exhibited type IV isotherms with H3 model hysteresis loops [34], indicating the presence of some mesopores. The inset shows the corresponding pore size distribution curves. The highest peak value of pore size distribution of VPO-pre-80 was about 33 nm, while that of VPO-pre-100 was about 40 nm. These pores should be formed by the accumulation of spherical particles. The pore size distribution of VPO-pre-80 was more concentrated and the pore volume was larger than that of VPO-pre-100, which is the reason why the specific surface area of VPO-pre-80 was higher than that of VPO-pre-100. The N_2 adsorption–desorption isotherms and pore size distribution curves for the final catalysts VPO-80 and VPO-100 after calcination of corresponding precursors in an n-butane/air atmosphere are shown in Fig. 2b. It can be seen that the type of isotherm and pore size distribution curve maintained the performance of the corresponding precursors and the pore size distribution of VPO-80 was still more concentrated than that of VPO-100. However, the pore volume of VPO-100 was larger than that of VPO-80, which indicates that part of the structural change occurred in the process of catalyst activation in the n-butane/air atmosphere.

3.3 XRD

The XRD patterns of VPO precursors synthesized in mixed solvents of ionic liquid and water in different proportions and pure water and pure ionic liquid are shown in Fig. 3a. It can be seen that when pure water was used as the solvent,

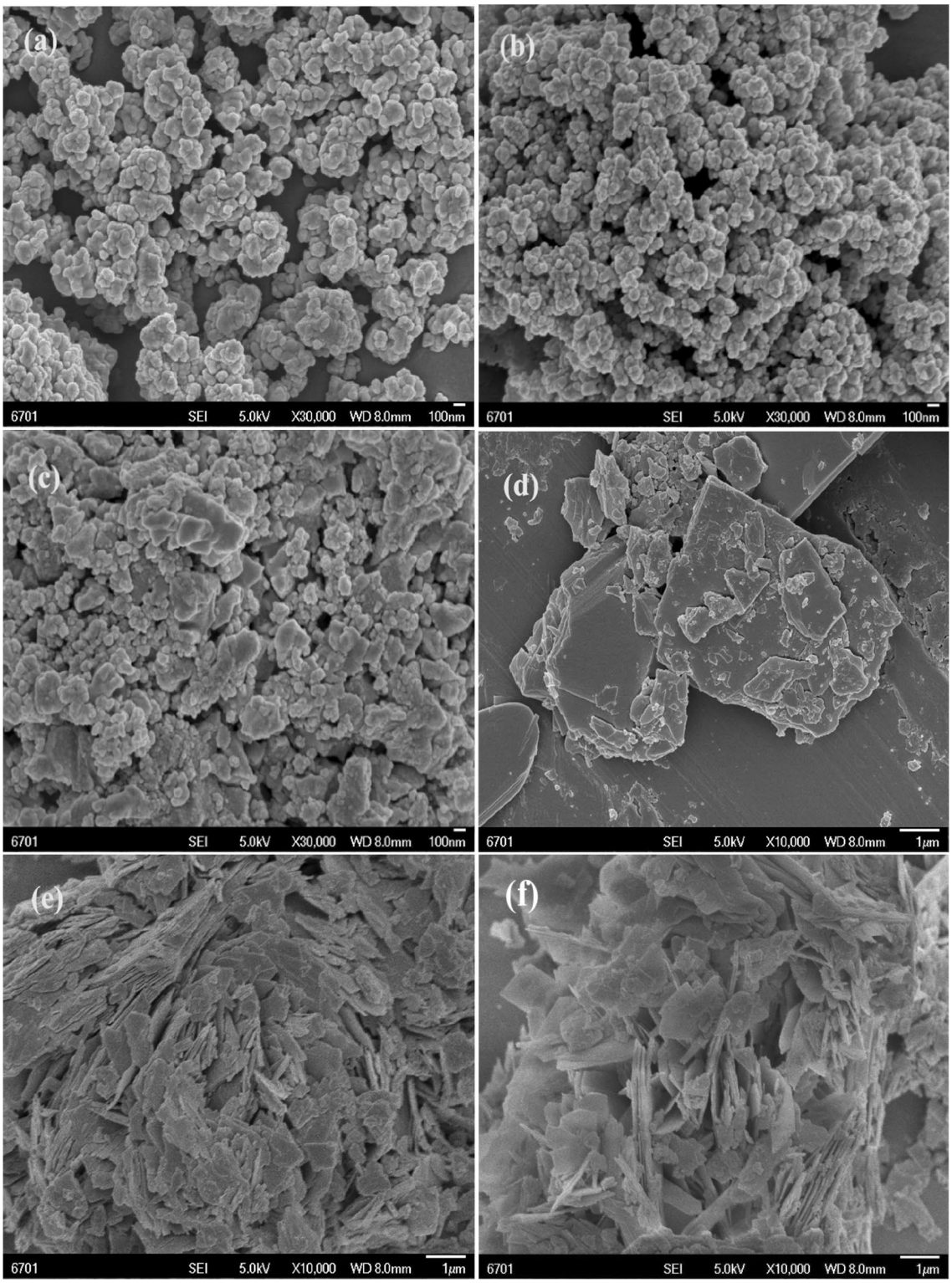

Fig. 1 SEM images of vanadium oxyphosphate (VPO) precursors prepared in mixed solvents of ionic liquid and water with different proportions: **a** VPO-pre-100, **b** VPO-pre-80, **c** VPO-pre-60, **d** VPO-pre-40, **e** VPO-pre-20 and **f** VPO-pre-0

Table 1 Textural properties of samples

Samples	Surface area (m^2/g)	Pore volume (cm^3/g)	Average Pore diameter (nm)
VPO-pre-0	9	0.04	20
VPO-pre-20	13	0.11	32
VPO-pre-40	12	0.32	10
VPO-pre-60	24	0.26	42
VPO-pre-80	59	0.47	32
VPO-pre-100	33	0.30	32
VPO-0	7	0.03	18
VPO-80	34	0.15	17
VPO-100	24	0.24	41

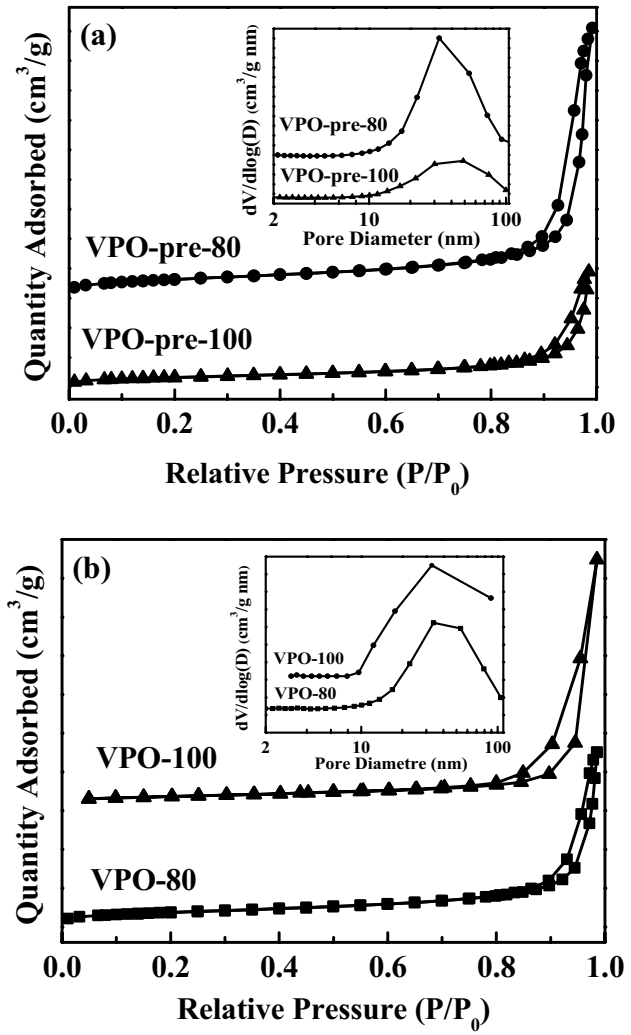

Fig. 2 N_2 adsorption–desorption isotherms of the precursor samples (**a**) and the final catalysts (**b**). Inset shows the corresponding pore size distributions

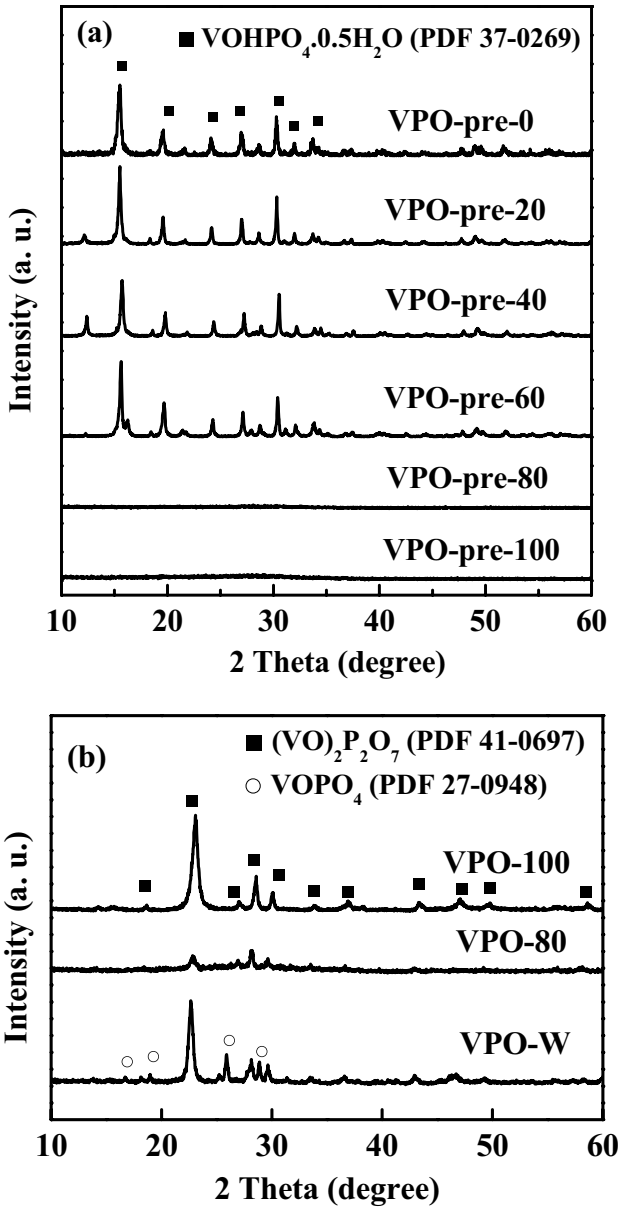

Fig. 3 XRD patterns of samples: **a** the precursors and **b** the final catalysts after calcination of the corresponding precursors in 1.2% n-butane/air atmosphere

the sample (VPO-pre-0) had sharp diffraction peaks at 2θ = 15.6, 19.6, 24.2, 27.1, 28.7 and 30.5°, which belong to the $VOHPO_4{\cdot}0.5H_2O$ crystal phase, indicating that the pure $VOHPO_4{\cdot}0.5H_2O$ crystal phase had been synthesized, which is consistent with the literature. When the ionic liquid was added to the solvent and the ratio was below 60%, the precursor was still mainly $VOHPO_4{\cdot}0.5H_2O$, except for a small amount of impurities with diffraction peak near 2θ = 12.5°. However, when the ratio of ionic liquid was more than 80% or pure ionic liquid was used, the crystal phase of the material changed greatly. The XRD spectrum only showed a

weak and wide diffraction peak between 20 and 40°, indicating that it was mainly an amorphous phase, which shows that ionic liquids have an important influence on the crystal phase of the synthesized materials. The SEM images above show that when the proportion of ionic liquid was less than 60%, all the obtained precursors contained lamellar structure morphology (a mixture of flakes and spherical particles at 60%), while the morphology of the precursor completely changed into uniform spherical particle morphology when the proportion of ionic liquid was 80% or pure ionic liquid (100%). Therefore, it can be inferred that the precursor with lamellar morphology may have been $VOHPO_4{\cdot}0.5H_2O$, while the spherical particles were amorphous.

Three typical samples (VPO-pre-0 synthesized in pure water solvent; VPO-pre-80, which had the highest specific surface area; and VPO-pre-100 synthesized in pure ionic liquid solvent) were calcined in an air mixture of 1.2% n-butane at 400 °C to obtain the final catalysts. The XRD results are shown in Fig. 3b. It can be seen that all the samples mainly changed into the $(VO)_2P_2O_7$ crystal phase, due to the intra-molecular dehydration process of hydrogen phosphate groups from the precursor (Although the precursor VPO-pre-100 was obtained in the pure ionic liquid solvent, the raw materials included H_3PO_3 and 85% H_3PO_4 solution, thus it is expected that the prepared VPO-pre-100 sample contained HPO_4^{2-} compounds or hydrogen-embed phosphates). There were sharp diffraction peaks at $2\theta = 22.9$, 28.4 and 29.9°, which belonged to the $(VO)_2P_2O_7$ crystal. The VPO-100 and VPO-80 phases were relatively pure, while the VPO-W phase was mainly $(VO)_2P_2O_7$ with a small amount of $VOPO_4$. At the same time, the diffraction peak intensity of VPO-100 was higher than that of VPO-80, which is consistent with the phenomenon that the particle size of the synthesized sample in pure ionic liquid was larger than that in a mixed solution of water and ionic liquid.

3.4 XPS

The composition and valence state of the chemical components on the catalyst surface were obtained using XPS; the analysis results are summarized in Table 2 and shown in Fig. 4. Figure 4a shows the XPS full spectrum of samples. Four characteristic peaks were observed at about 285.0, 517.5, 531.6, and 133.9 eV, representing the chemical characteristics of C 1 s, V 2p, O 1 s, and P 2p orbits, respectively.

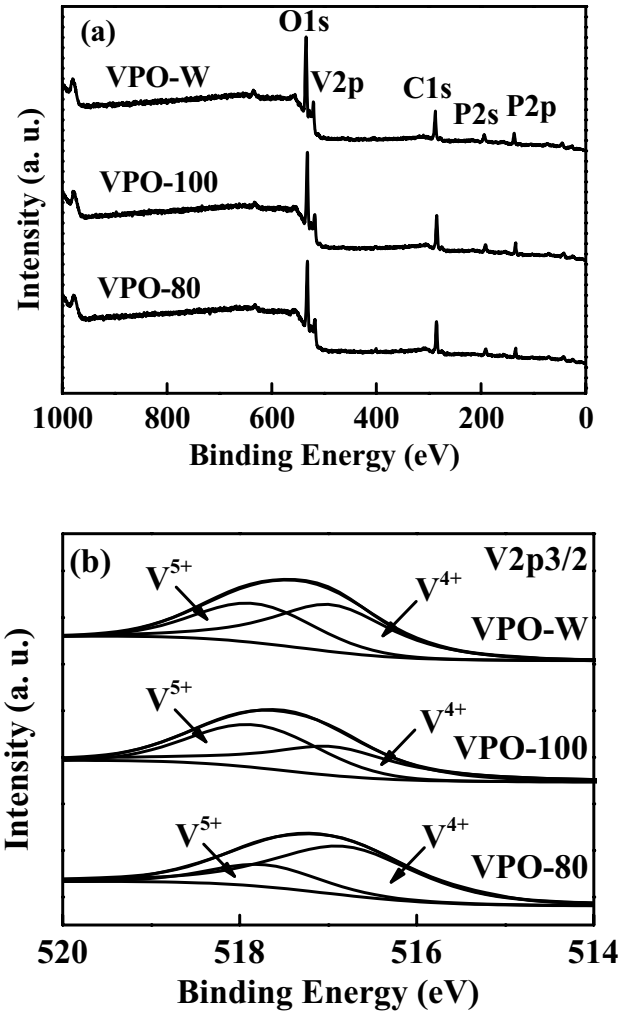

Fig. 4 The XPS spectra for the typical final catalysts: **a** full spectrum and **b** V $2p_{3/2}$

The carbon component was the external calibration phase, so it did not belong to the composition of this sample. The results from Fig. 4b and Table 2 show that the surface P/V atomic ratio of the three samples was different—1.07 for VPO-W, while that for VPO-100 and VPO-80 were both less than 1, at 0.98 and 0.78, respectively, which once again reflects the difference between water solvent synthesis and ionic liquid synthesis. The V $2p_{3/2}$ BEs of VPO-100 and VPO-80 were 517.6 eV and 517.2 eV, respectively, which are higher than that of a well-crystallized $(VO)_2P_2O_7$

Table 2 XPS data of the VPO catalysts

Catalyst	BE (eV)			Surface concentration (at%)				P/V atomic ratio	V^{4+}/V^{5+}
	V 2p	P 2p	O 1 s	C	O	P	V		
VPO-80	517.2	133.7	531.6	40.51	42.98	7.23	9.27	0.78	2.00
VPO-100	517.6	134.0	531.9	44.38	39.25	8.10	8.27	0.98	1.01
VPO-W	517.5	133.9	531.5	36.53	45.79	9.13	8.55	1.07	1.35

(516.6 eV), but lower than that for vanadium phosphate material [13]. The curve-fitting analysis for V $2p_{3/2}$ BE curves for different catalysts is shown in Fig. 4b. The surface atomic ratio of V^{4+} to V^{5+} species were estimated through curve-fitting analysis and the results are shown in Table 2. The VPO-80 catalyst possessed the highest V^{4+}/V^{5+} ratio of about 2.00, and that for the VPO-100 and VPO-W catalysts were 1.01 and 1.35, respectively, which coincide well with the XRD patterns with $(VO)_2P_2O_7$ as the main phase.

3.5 Catalytic Performances

The catalytic oxidation of cyclohexanol to cyclohexanone was chosen as the probe reaction to evaluate the catalytic performances. The catalytic performance of three typical catalysts (VPO-W, VPO-80, VPO-100) was compared. First, the VPO-80 catalyst with the highest specific surface area was used to optimize the process conditions.

The effects of reaction temperature on the conversion of cyclohexanol and the selectivity for cyclohexanone using the VPO-80 catalyst at a reaction time of 2 h with a molar ratio of H_2O_2 to cyclohexanol of 6 are shown in Fig. 5. It can be seen that with the increase of reaction temperature, the conversion of cyclohexanol first increased and then decreased. When the reaction temperature was 70 °C, the highest conversion of cyclohexanol was 69.60%. However, the conversion of cyclohexanol decreased with the increase of reaction temperature, probably due to the thermodynamic equilibrium control under the exothermic reaction and the hydrogen peroxide decomposition at high temperatures [35]. The selectivity for cyclohexanone also first increased and then decreased with the increase of reaction temperature. When the reaction temperature reached 70 °C, the selectivity of the target product reached 83.31%. When the reaction temperature was further increased, the selectivity for cyclohexanone decreased, possibly due to a side reaction at the higher reaction temperature. Therefore, the optimum reaction temperature was 70 °C.

The effects of different molar ratios of H_2O_2 to cyclohexanol on the conversion of cyclohexanol and the selectivity for cyclohexanone using the VPO-80 catalyst at a reaction time of 2 h at 70 °C are shown in Fig. 6. Without the addition of H_2O_2, the conversion of cyclohexanol was nearly zero, which indicated that the reaction cannot occur without the oxidant at the current reaction conditions. When the molar ratio of H_2O_2 to cyclohexanol was 2, the conversion of cyclohexanol was sharply increased to 25.37%, which indicated that the H_2O_2 is an effective oxidant for this reaction. With an increase in the amount of H_2O_2, the conversion rate of cyclohexanol gradually increased. When the molar ratio of H_2O_2 to cyclohexanol reached 6, the highest conversion of cyclohexanol was obtained at 69.60%. When the amount of H_2O_2 was further increased, the conversion of cyclohexanol remained almost unchanged, but the selectivity for cyclohexanone gradually decreased. The reason is that with an increase of H_2O_2 dosage, cyclohexanone was further oxidized to other by-products under the combined action of hydrogen peroxide and catalyst, which affects the selectivity for cyclohexanone. Considering the conversion of cyclohexanol and the selectivity for cyclohexanone, a molar ratio of H_2O_2 to cyclohexanol of 6 is optimum.

The effects of different reaction times on the conversion of cyclohexanol and the selectivity for cyclohexanone using the VPO-80 catalyst were also studied at 70 °C with

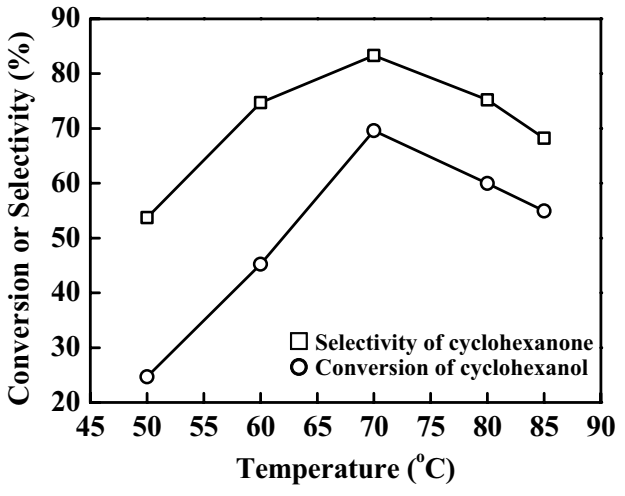

Fig. 5 The effects of reaction temperature on the conversion of cyclohexanol and the selectivity for cyclohexanone for the reaction time 2 h with the molar ratio of H_2O_2 to cyclohexanol of 6 over the VPO-80 catalyst

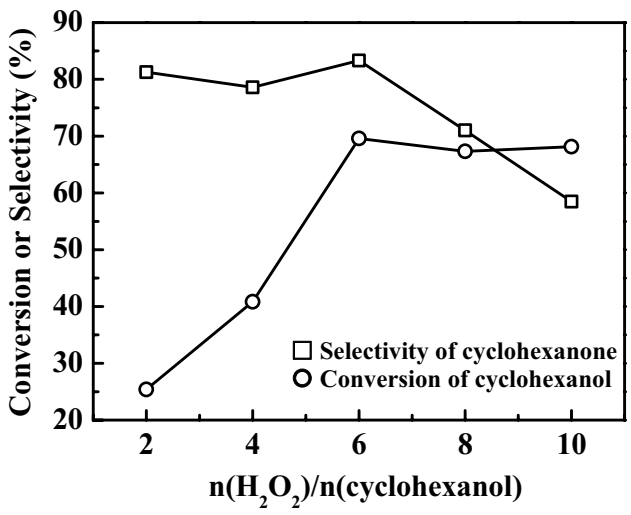

Fig. 6 The effects of different molar ratios of H_2O_2 to cyclohexanol on the conversion of cyclohexanol and the selectivity for cyclohexanone for the reaction time 2 h at 70 °C over the VPO-80 catalyst

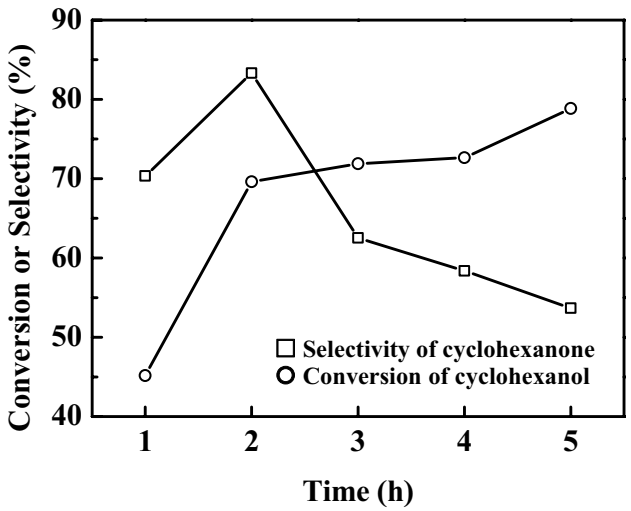

Fig. 7 The effects of different reaction times on the conversion of cyclohexanol and the selectivity for cyclohexanone at 70 °C and the molar ratio of H_2O_2 to cyclohexanol of 6 over the VPO-80 catalyst

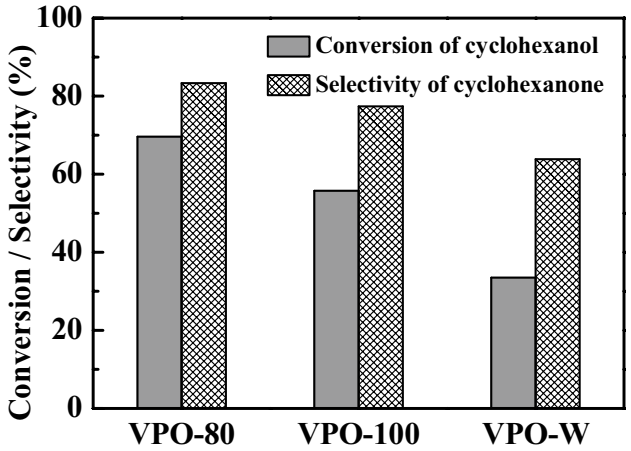

Fig. 8 The catalytic performance of three typical catalysts for the selective oxidation of cyclohexanol to cyclohexanone under the optimized reaction conditions

a molar ratio of H_2O_2 to cyclohexanol of 6, and the result is shown in Fig. 7. With the extension of reaction time, the conversion of cyclohexanol continued to increase, but the increase slowed after 2 h. At the same time, the selectivity for cyclohexanone decreased sharply after 2 h. Thus, the optimum reaction time was 2 h.

In addition, a blank reaction without catalyst was also carried out. With a molar ratio of H_2O_2 to cyclohexanol of 6, the reaction temperature at 70 °C and reaction time at 2 h, the conversion of cyclohexanol was only 1.78%, which indicated that the VPO catalysts could indeed accelerate the oxidation reaction greatly.

Based on the above optimized reaction conditions, the catalytic performance of three typical catalysts for the selective oxidation of cyclohexanol to cyclohexanone was compared. The results are shown in Fig. 8. The conversion of cyclohexanol was 69.60% and 55.72%, and the selectivity for cyclohexanone was 83.31% and 77.34%, respectively, for the VPO-80 and VPO-100 catalysts synthesized using an ionothermal method. The conversion of cyclohexanol and selectivity for cyclohexanone were 33.51% and 63.88%, respectively, for the VPO-W catalyst synthesized using the hydrothermal method. The final yield of cyclohexanone using the VPO-80 catalyst system was 57.98%, while that for the VPO-W catalyst system was only 21.41%, which shows the advantages of a catalyst synthesized using an ionothermal method with high surface areas, small spherical particle morphologies, low surface P/V ratios and so on.

4 Conclusions

A series of VPO catalyst precursors was synthesized using H_3PO_3 as a reducing agent and partial phosphorus source, H_3PO_4 as an additional phosphorus source, V_2O_5 as the vanadium source, and a mixed solution of ionic liquid and water with different volume ratios as the reaction solvent. The effect of ionic liquid ratio on VPO precursors was investigated in detail. SEM results show that the precursor of the VPO-W catalyst synthesized using a hydrothermal method, with deionized water as the reaction solvent, is a large and flaky compound. With the increase of the proportion of ionic liquid, the size of the large flakes gradually decreased, and the morphology was changed to spherical particles. When the proportion of ionic liquid was 80% or the solvent was pure ionic liquid (100%), the VPO precursors were small and completely spherical particles. The BET surface area of precursor VPO-pre-80 was high at 59 m^2/g, while that of VPO-pre-0 obtained in pure water solvent was only 9 m^2/g. The XRD results showed that when the volume ratio of ionic liquid to water was less than 60%, the precursor of the VPO catalyst mainly existed in the $VOHPO_4{\cdot}0.5H_2O$ crystal phase. When the volume ratio of ionic liquid reached 80%, the precursor of the VPO catalyst changed from $VOHPO_4{\cdot}0.5H_2O$ to an amorphous state. All of the above results show that ionic liquids play an important role in the synthesis of VPO materials. After being calcined at high temperature in an air mixture containing 1.2% n-butane, all of the VPO precursors were transformed into the vanadium pyrophosphate phase, which was used in the selective oxidation of cyclohexanol to cyclohexanone by the final catalysts. The yield of cyclohexanone was 57.98% using a VPO-80 catalyst synthesized by an ionothermal method, while it was only 21.41% in the selective oxidation reaction of cyclohexanol using a VPO-W catalyst synthesized by a traditional

hydrothermal method, which shows the great advantages of VPO catalysts synthesized in an ionic liquid solvent.

Acknowledgements Financial supports from National Natural Science Foundation of China (Grant No. 21763016) and Industrial Support Program for colleges and universities in Gansu Province (Grant No. 2020C-06) are acknowledged.

Compliance with Ethical Standards

Conflict of interest The authors declare that they have no known competing financial interests or personal relationships that could have appeared to influence the work reported in this paper.

References

1. Lashier ME, Schrader GL (1991) J Catal 128:113–115
2. Liu J, Wang PC, Feng YN, Xu ZJ, Feng XZ, Ji WJ, Au CT (2019) J Catal 374:171–182
3. Ivars-Barceló F, Hutchings GJ, Bartley JK, Taylor SH, Sutter P, Amorós P, Sanchis R, Solsona B (2017) J Catal 354:236–249
4. Hutchings GJ (1991) Appl Catal 72:1–32
5. Wang F, Dubois JL, Ueda W (2010) Appl Catal A Gen 376:25–32
6. Li GX, Zhang Q, Fang WG, Zhao Y (2015) Energy Environ Focus 4:301–306
7. Hutchings GJ (2004) J Mater Chem 14:3385–3395
8. Cheng MJ, Goddard WA (2013) J Am Chem Soc 135:4600–4603
9. Dietl N, Wende T, Chen K, Jiang L, Schlangen M, Zhang X, Asmis KR, Schwarz H (2013) J Am Chem Soc 135:3711–3721
10. Schulz C, Roy SC, Wittich K, Naumann d'Alnoncourt R, Linke S, Strempel VE, Frank B, Glaum R, Rosowski F (2019) Catal Today 333:113–119
11. He B, Li ZH, Zhang HL, Dai F, Li K, Liu RX, Zhang SJ (2019) Ind Eng Chem Res 58:2857–2867
12. Leong LK, Chin KS, Taufiq-Yap YH (2012) Appl Catal A Gen 415–416:53–58
13. Feng XZ, Yao Y, Su Q, Zhao L, Jiang W, Ji WJ, Au CT (2015) Appl Catal B Environ 164:31–39
14. Hutchings GJ, Kiely CJ, Sananesschulz MT, Burrows A, Volta JC (1998) Catal Today 40:273–286
15. Feng XZ, Sun B, Yao Y, Su Q, Ji WJ, Au CT (2014) J Catal 314:132–141
16. Harrouch-Batis N, Batis H, Ghorbel A, Vedrine JC, Volta JC (1991) J Catal 128:248–263
17. Hutchings GJ, Sananes MT, Sajip S, Kiely CJ, Burrows A, Ellison IJ, Volt JC (1997) Catal Today 33:161–171
18. Carreon MA, Guliants VV, Pierelli F, Cavani F (2004) Catal Lett 92:11–16
19. Otaibi RA, Weng WH, Bartley JK, Dummer NF, Kiely CJ, Hutchings GJ (2010) ChemCatChem 2:443–452
20. Lopez-Sanchez JA, Griesel L, Bartley JK, Wells RPK, Liskowski A, Su DS, Schlögl R, Volta JC, Hutchings GJ (2003) Phys Chem Chem Phys 5:3525–3533
21. Cooper ER, Andrews CD, Wheatley PS, Webb PB, Wormald P, Morris RE (2004) Nature 430:1012–1016
22. Liu H, Tian ZJ, Wang L, Wang YS, Li DW, Ma HJ, Xu RS (2016) Inorg Chem 55:1809–1815
23. Liu L, Yang J, Li JP, Dong JX, Šišak D, Luzzatto M, McCusker LB (2011) Angew Chem Int Ed 50:8139–8142
24. Parnham ER, Morris RE (2007) Accounts Chem Res 40:1005–1013
25. Zhu HG, Huang JF, Pan ZW, Dai S (2006) Chem Mater 18:4473–4477
26. Yang G, Li LH, Wu C, Humphrey MG, Zhang C (2019) Inorg Chem 58:12582–12589
27. Wagle DV, Zhao H, Baker GA (2014) Accounts Chem Res 47:2299–2308
28. Wang GM, Valldor M, Siebeneichler S, Wilk-Kozubek M, Smetana V, Mudring AV (2019) Inorg Chem 58:13203–13212
29. Tan DM, Wang FX, Pietsch T, Grasser MA, Doert T, Ruck M (2019) ACS Appl Energy Mater 2:5140–5145
30. Chen D, Liu TT, Wang PY, Zhao JH, Zhang CT, Cheng RL, Li WQ, Ji PX, Pu ZH, Mu SC (2020) ACS Energy Lett 5:2909–2915
31. Wang GM, Valldor M, Dorn KV, Wilk-Kozubek M, Smetana V, Mudring AV (2019) Chem Mater 31:7329–7339
32. Xue YX, Chen JL, Shao J, Han LQ, Li WL, Sui CH (2020) Mol Catal 492:111010
33. Parnham ER, Morris RE (2006) Chem Mater 18:4882–4887
34. Mao Y, Duan H, Xu B, Zhang L, Hu YS, Zhao CC, Wang ZX, Chen LQ, Yang YS (2012) Energy Environ Sci 5:7950–7955
35. Li XX, Li CQ, Wang RJ, Chen SN, Zhao SJ, Kong XB (2019) Chem Adhes (China) 41:240–269

Affiliations

Yu Zhao[1] · Weiwei Zhang[1] · Shidong Wang[1] · Peng Dong[1] · Guixian Li[1] · Jianyi Shen[2]

✉ Yu Zhao
yzhao@lut.edu.cn

[1] Present Address: School of Petrochemical Engineering, Lanzhou University of Technology, Lanzhou 730050, Gansu, China

[2] School of Chemistry and Chemical Engineering, Nanjing University, Nanjing 210093, Jiangsu, China